RSC Advances

ROYAL SOCIETY OF CHEMISTRY

www.rsc.org/advances

Morphology dependent nanosecond and ultrafast optical power limiting of CdO nanomorphotypes

Paulose Thomas, [a] *P. Sreekanth* [b], *Reji Philip* [b] *and Abraham K.E* [a*]

[a] Department of Physics, St.Berchmans College, Changanassery 686 101, India

[b] Light and Matter Physics Group, Raman Research Institute, C.V.Raman Avenue, Sadashivanagar, Bangalore 560 080, India

[*]CORRESPONDING AUTHOR E-mail: abrahamke@gmail.com; Tel: +919447406915

ABSTRACT: A versatile approach to the fabrication of cadmium oxide (CdO) nanospheres, nanoflakes and nanoparallelepiped shapes through chemical precipitation and hydrothermal methods are studied. The growth mechanism of nanostructures is elucidated on the basis of capping agent and reaction time. The crystalline nature and various geometrical shapes of nanostructures are examined by X-ray diffraction and high resolution transmission electron microscopic analysis. Nonlinear optical absorption and optical power limiting studies of nanostructures are carried out using open aperture Z-scan technique in the nanosecond (ns) and femtosecond (fs) excitation time scales. Optical nonlinearity is found to be arising from effective two- photon absorption involving excited state absorption. The magnitude of effective two-photon absorption coefficient is calculated and found to be in the range of 10^{-10}m/W for ns and 10^{-15} m/W for fs. The nonlinear optical study discloses that the nonlinear optical absorption and optical limiting threshold values are strongly related to nanomaterial morphology. The Brunauer-Emmett-Teller (BET) surface area analysis also confirms our claim that the optical nonlinearity is strongly dependant on the morphology as well as surface area of the nanomaterial. Thus the present nanomorphotypes have potential applications in devices for optical limiting, optical switching, pulse shaping, pulse compression and optical diode action.

KEYWORDS: *Hydrothermal, Growth mechanism, Nano and femto second, Nonlinear optical absorption*.

1. INTRODUCTION

Nanostructures with distinguished morphologies have received great attention in recent years for their potential applications in the areas of nanofabrication, optoelectronic nanodevices and biological imaging and sensing applications. [1, 2] Metal oxide nanostructures with various geometric shapes have been received great attention due to their unique physical, chemical, electrical, optical and magnetic properties. Recent studies on metal oxide nanostructures have been mainly focused on the synthesis of regular morphologies such as tubes, rods, wires, cubes, triangle and flower, etc through different chemical methods.[3, 4] However cost effective single step production of various nanomorphotypes with high yield and reproducibility still remains an important problem. CdO nanostructures have been extensively studied in the past few decades, which have been used as an interconnection in a wide variety of commercial applications particularly in photonics.[5, 6] CdO is an n-type IIB-VIA, semiconductor with direct band gap of 2.5 eV and indirect band gap of 1.98 eV.[7, 8] In the recent years many researchers have focused on synthesis of CdO nanomaterials in various morphotypes, because of its promising applications in optoelectronics, gas sensing, solar cells and flat panel displays.[9, 10] Therefore people have much interest to study its optical property especially in nonlinear optical analysis. Nonlinear optics is one of the leading areas of research in nanomaterial for its importance in optical switching, optical limiting, photo-thermal cancer therapy, and sensor and eye protection.[11, 12] An ideal optical limiter is a devise which satisfy the lower limiting threshold, high optical damage threshold, faster response time, chemical and environmental stability and higher linear transmittance.[13, 14] Recent literatures have revealed various fabrications of hierarchical structures of CdO nanomaterials like nanowires, nanosheets, nanorods, nanobelts, and nanoparticles. For example T. Ghoshal et al. present the synthesis of CdO nanostructures in

hexagonal sheet and rods.[15] Fabrication of CdO microspheres through Ostwald ripening method was developed by wang et al.[16] N.A.M Barakat et al. illustrated the photoluminescence and optical characterization of CdO nanorods.[17] Jia et. al. fabricated porous CdO nanostructures like nanowires, nanobelts, nanorolls and one dimensional hierarchical structures.[18] But very little literatures are available for the nonlinear optical properties of various CdO nanomorphotypes. The only report on nonlinear study of CdO nanomaterial is of Q. Chang et al. who elucidates the optical limiting property of CdO nanowires in ethanol and water suspensions and concluded that the optical limiting property is due to nonlinear scattering.[19] Many researchers have studied the optical limiting property of nanostructures with various morphotypes. For example, Pan et al. presented the nonlinear analysis of Pd, Cu, Ni, Pt, Ag and Co nanowires.[20] V.S. Muthukumar et al. and Gao et al. conducted the study on optical limiting property of CdS nanowires and C_{60} TPY-Pb nanowires.[21, 22] In this article, we investigate the nonlinear optical absorption and optical limiting properties of three different CdO nano morphotypes synthesized through chemical precipitation and hydrothermal method, which are well dispersed in ethanol. This is the first ever made report of the fabrication of CdO nanoflakes and nanoparallelepiped geometrical shape as well as its nonlinear optical properties. The laser pulse energy of 532 nm used in the nonlinear analysis is the near-resonant excitation region. Results reveal that the major contribution of nonlinear absorption mechanism is due to effective two-photon absorption process (TPA). The nonlinear optical properties of the present morphologies are compared with the previous results which reveals that the prepared CdO morphotypes especially nanosphere are better candidate for optical limiting purposes.

2. RESULTS AND DISCUSSION

2.1 Structural Analysis: A representative XRD spectrum of CdO nanosphere, nanoflakes and nanoparallelepiped morphotypes are given in Fig. 1a, 1b and 1c respectively. The XRD data are further refined by a quantitative analysis performed by match! 2 Rietveld method as shown in Fig. 2. The diffraction peaks of the samples are very sharp and highly intense which reveals the well defined crystalline nature, phase purity and lack of impurities in the prepared nanostructures. The diffraction pattern of CdO at (111), (200), (220), (311) and (222) planes matches well with the JCPDS card No. 05-0640 of CdO with lattice constant a=4.695 A^0. The intensity of (111) plane is particularly strong compared with the other peaks, suggesting that the CdO nanostructures grow on (111) crystal plane which exactly match with the HRTEM analysis of the same material. The average crystallite size of the sample is calculated by Scherrer's formula and found to be 15 nm for spherical shape, 17 nm for nanoflakes and 20 nm for parallelepiped morphotypes.

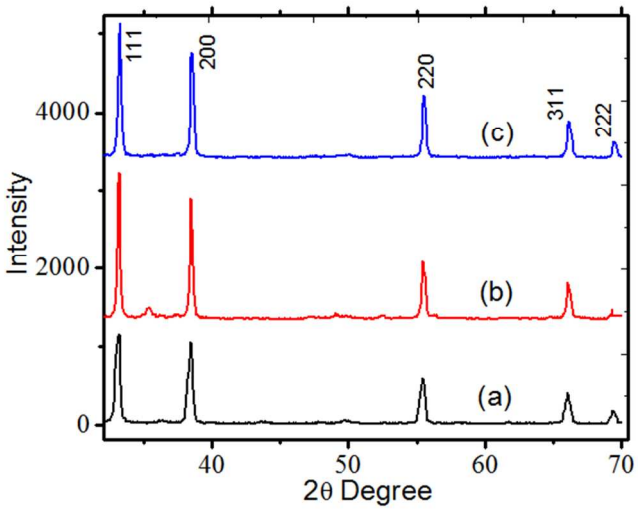

Figure 1. XRD spectrum of CdO nanomorphotypes; (a) Nanosphere, (b) Nanoflakes and (c) Nanoparallelepiped.

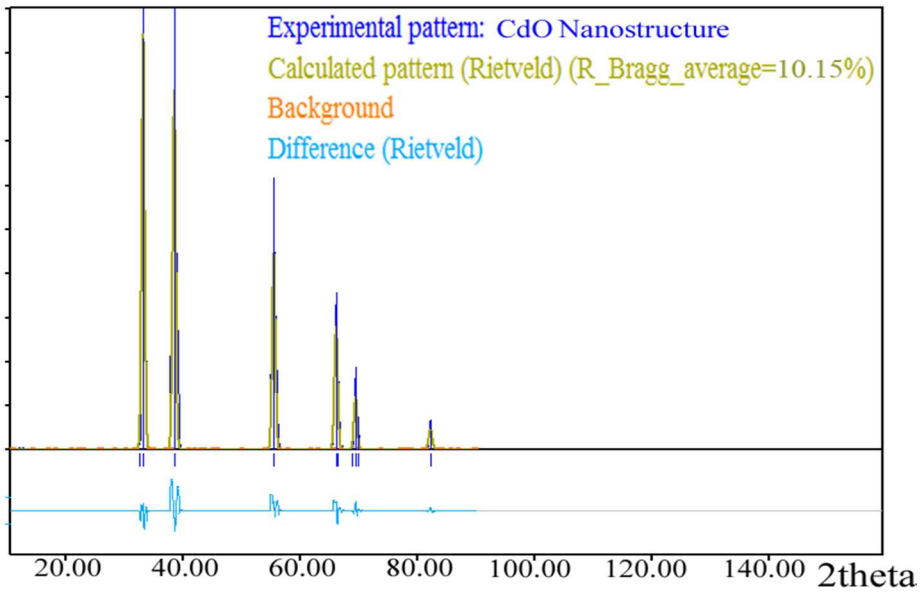

Figure 2. Rietveld refined result of CdO nanostructure (R factor =10.15%).

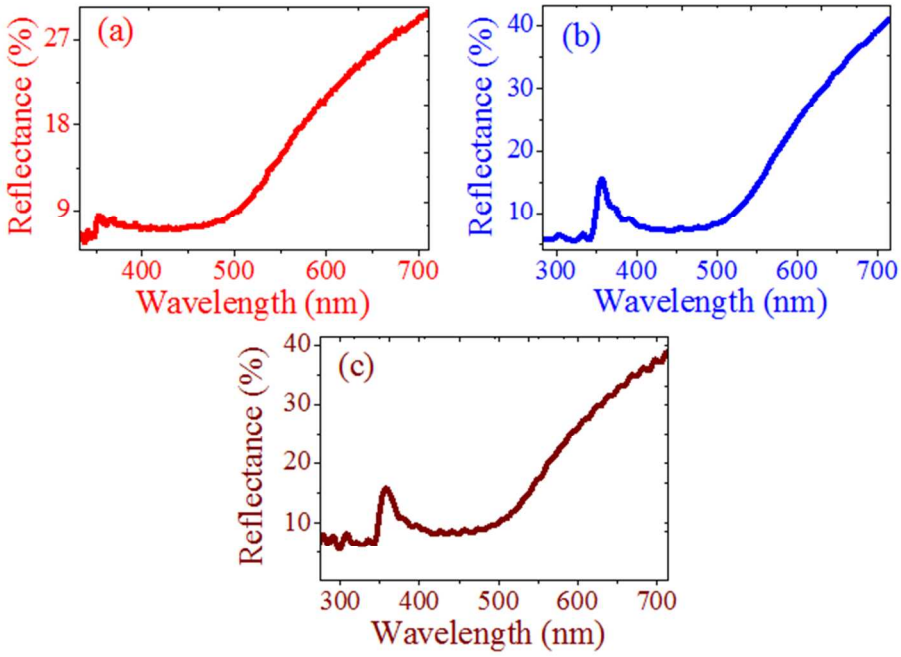

Figure 3. UV-Vis reflectance spectrum of CdO nanomorphotypes; (a) Nanosphere, (b) Nanoflakes and (c) Nanoparallelepiped.

2.2 UV-Visible Spectroscopy: The UV-Visible reflectance spectrums of CdO nanosphere, nanoflakes and nanoparallelepiped morphotypes recorded are depicted in Fig. 3a, 3b and 3c respectively within the wavelength range of 200-800 nm. The relation between the linear optical absorption coefficient (α) and the photon energy (hν) can be written as

$$(\alpha h\nu)^{1/n} = B(h\nu - E_g) \qquad (1)$$

Where B is a constant and E_g is the optical bandgap of materials. The exponent 'n' is a constant which depends on the type of transitions. To determine the possible transitions, $(\alpha h\nu)^{1/n}$ versus (hν) graph is plotted and band gap is determined by extrapolating the linear portion of the graph on (hν) axis . The direct bandgap is obtained by fitting the experimental data to the eq. 1with n=1/2 for each structure and are presented in the Table 1. The optical bandgap obtained is maximum in the case of CdO nanosphere compared to other morphologies.

Table 1. Crystallite size and direct band gap of CdO morphotypes

Morphotypes	Crystallite size (nm)	Direct band gap (eV)
Spherical	15	2.75
Flakes	17	2.62
Parallelepiped	20	2.52

Table 2. EDS analysis of CdO nano morphotypes.

Elements	Atomic (%)	Formula
Nanosphere		CdO
Cadmium	50.00	
Oxygen	50.00	
Nanoflakes		CdO
Cadmium	50.00	
Oxygen	50.00	
Nanoparallelepiped		CdO
Cadmium	50.00	
Oxygen	50.00	

2.3 Morphology: Fig. 4 depicts the SEM and HRTEM images of CdO morphotypes, which inveterate the versatile morphology of CdO nanostructures. Fig. 4a, 4b and 4c expounds the SEM images of precursor nanosphere, nanoflakes and nanoparallelepiped morphotypes. Fig. 4d, 4e and 4f show the HRTEM images of nanosphere, nanoflakes and nanoparallalepiped structures. Its corresponding SAED patterns are presented in the inset of Fig. 4a, 4b and 4c respectively. The SAED patters clearly confirm the defect free and well defined face centered cubic crystal structure of CdO material. Size dimensions of morphotypes are measured from HRTEM images and are of the order of 20 nm for sphere, 45 for flakes and 56 for parallelepiped. Inset of 4d, 4e and 4f is helpful to understand the clear morphology of a single sphere, flake and parallelepiped nanostructure and also its size dimensions.

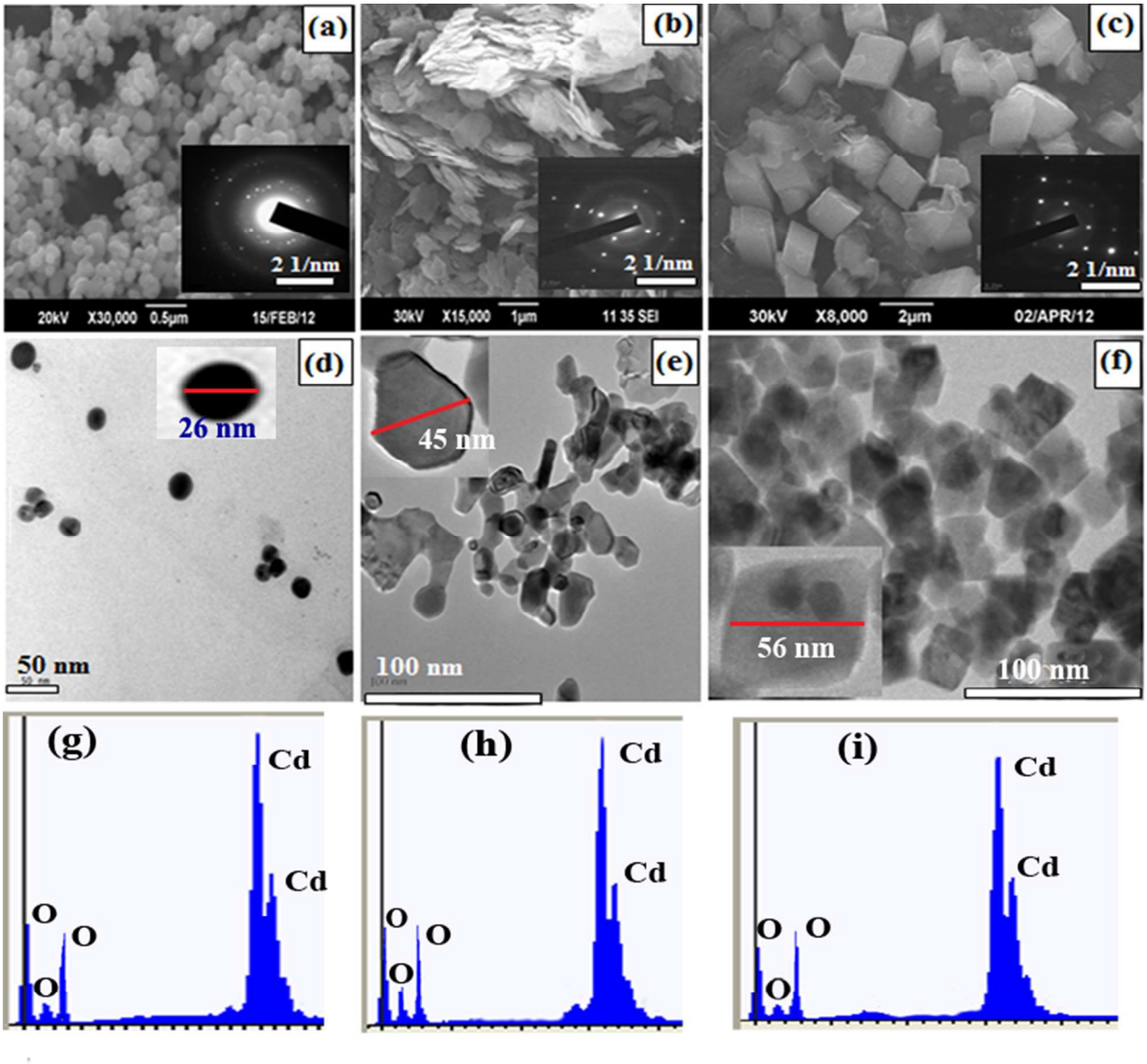

Figure 4. SEM and HRTEM images of CdO nanomorphotypes; (a), (b) and (c) are the SEM images of nanosphere, nanoflakes and nanoparallelepiped morphotypes and corresponding HRTEM SAED pattern (inset) respectively. (d), (e) and (f) are the HRTEM images of nanosphere, nanoflakes and nanoparallelepiped structures. Inset of (d), (e) and (f) shows enlarged view of a single sphere, nanoflake and nanoparallelepiped shape. (g), (h) and (i) are the EDS spectrum of nanosphere, nanoflakes and nanoparallelepiped morphotypes respectively.

The EDS spectrum of spherical, flakes and parallelepiped morphotypes are given in Fig. 4g, 4h and 4i respectively which detect only the Cd and O signals, suggesting that as obtained CdO morphotypes consists of Cd and O elements with 50:50 atomic %. Atomic percentage of Cd and O obtained from EDS analysis for all nanomorphotypes are presented in Table 2.

2.4 Nonlinear Optical analysis: The open aperture z-scan technique [23] is used to carry out nonlinear transmission measurements, which is essentially a measurement of the optical transmission of the sample as a function of input light intensity. The setup for z-scan consists of a pulsed laser beam of known energy, a converging lens to focus the laser beam, and a laser energy detector. The propagation direction of the laser beam is assumed to be in the z-axis, such that the fluence is maximum at the focal point z =0 which decreases towards either direction on the z-axis. The sample is moved along the z-axis, towards or away from the focal point to vary the light fluence falling on it. The position versus transmission curve (z-scan curve) can be drawn by measuring the transmitted energy for different sample positions using a detector. Optical nonlinearity coefficients can then be calculated numerically by fitting the measured Z-scan curve to standard nonlinear optical transmission equations. The laser sources used in the current setup is a Q-switched Nd:YAG laser (Minilite, continuum Inc) emitting at the second harmonic wavelength of 532nm and a regeneratively amplified Ti:Supphire amplifier operating at the wavelength of 800nm. The Gaussian beam was focused through a plano- convex lens of focal length 10.75 cm. The laser pulse widths (FWHM) are approximately 5ns and 100fs at 532nm and 800nm respectively. The powder samples are suspended in ethanol by sonication and are then taken in a 1 mm cuvette. The cuvette is mounted on a stepper motor controlled linear translational stage and is translated along the z-axis through the focal region. The sample sees

different laser fluences at each z positions, and the corresponding transmissions are measured using a pyroelectric energy probe (Rj7620, Laser probe Inc.) placed after the sample.

Table. 3 Nonlinear absorption coefficient (β_{eff}) and Saturation intensity (I_S) for ns and fs excitations, obtained by numerical fits to the data points using eq. 3.

Morphotypes	**532nm, 5ns excitation.**			**800nm, 100fs excitation.**		
	energy μJ	β_{eff} ($x10^{-10}$ m/W)	I_S ($x10^{12}$ W/m^2)	energy μJ	β_{eff} ($x10^{-15}$ m/W)	I_S ($x10^{16}$ W/m^2)
Spherical	100	2	2.0	10	7.1	3
Flakes	100	0.98	4.9	10	6.9	3.5
Parallelepiped	100	0.73	5.9	10	4	9.8

The reason for optical limiting property of a semiconductor nanomaterial is either nonlinear absorption or nonlinear scattering, or both. Undoped semiconductor materials reveal free carrier absorption at a wavelength of linear absorption, but they show two-photon absorption at wavelengths away from the linear absorption region.[24] Fig. 5a-c shows the open aperture z-scan (inset) and corresponding fluence dependent nonlinear optical transmission obtained in the nanosphere, nanoflakes and nanoparallelepiped morphotypes respectively for 532nm, 5ns excitation at the input laser pulse energy of 100 μJ, whereas Fig. 6a-c represent that for 800nm, 100fs excitation at an input laser pulse energy of 10 μJ. The observed data are fitted to theoretical models and it is found that the process involves effective two photon absorption

(2PA) along with saturable absorption (SA). The intensity dependent nonlinear absorption coefficient $\alpha(I)$ is given by [25]

$$\alpha(I) = \frac{\alpha_0}{1 + \left(I / I_s \right)} + \beta_{eff} I \qquad (2)$$

Where α_0 is the unsaturated linear absorption coefficient at the excitation wavelength, I is the input laser intensity, I_S is the saturation intensity and β_{eff} is the effective two-photon absorption coefficient. The transmitted intensity for a given input intensity is calculated numerically by solving the corresponding propagation equation,

$$\frac{dI}{dz'} = -\left[\alpha_0 \Big/ \left(1 + \frac{I}{I_S} \right) + \beta_{eff} I \right] I \qquad (3)$$

where z' indicates the propagation distance within the sample. In open-aperture z-scan curves, valleys indicate a decrease in transmission, while peaks indicate an increase in transmission. The open circles are the observed data points and solid lines are the theoretical fits to the data points using eq. 3. The obtained nonlinear absorption coefficients values are presented in Table 3. Here one of the excitation energy 2.33 eV (corresponding to 532nm) used for z-scan measurement is near-resonant excitation, which is clear from our UV-Vis reflectance spectrum. From the reflectance spectra (Fig. 3), it can be seen that all the samples show some reflection between 560 nm to 650 nm. In the case of near-resonant excitation both two-photon absorption and excited state absorption will occur, and the process is collectively called effective two-photon absorption.

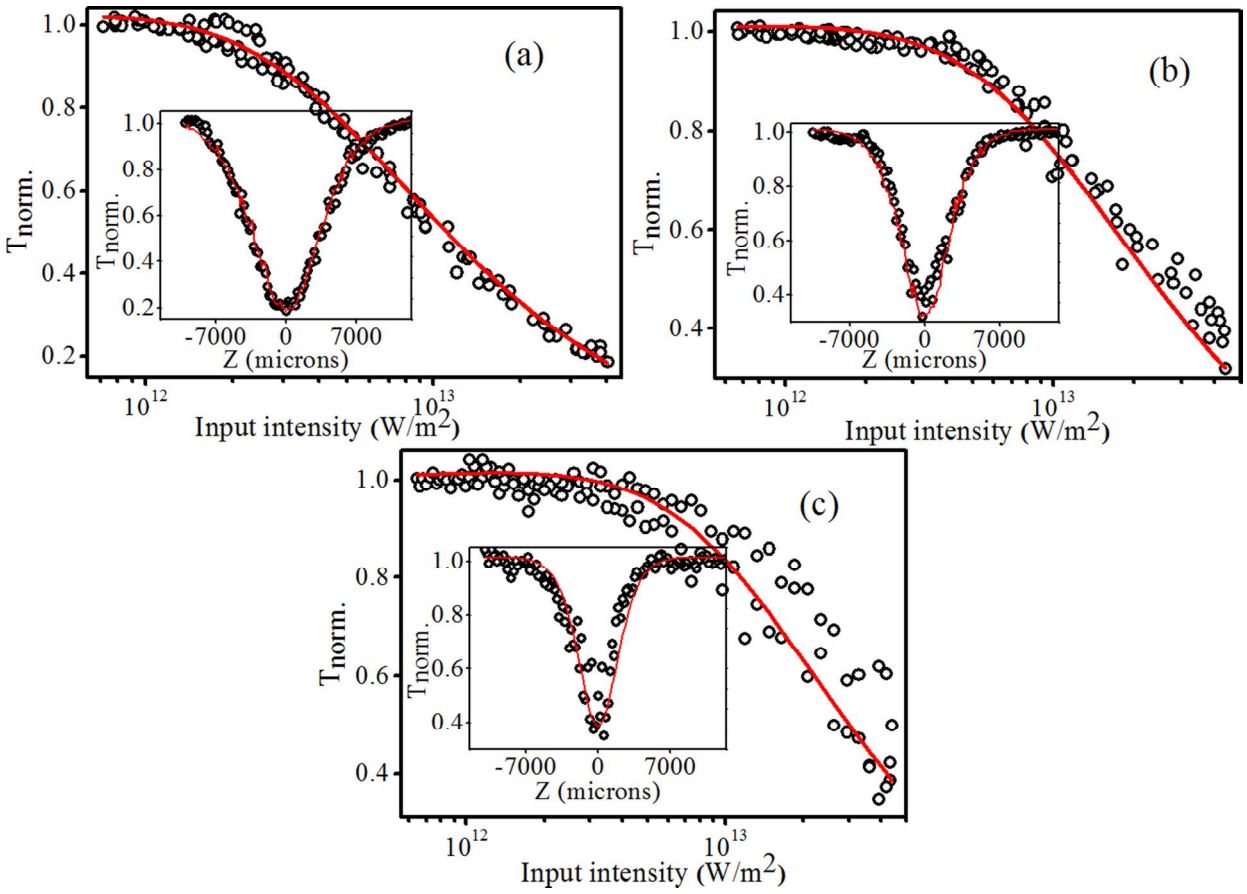

Figure 5. Open aperture Z-scans (inset) and optical limiting curves for the CdO nanomorphotypes for 532nm, 5ns laser pulse excitation at laser pulse energy of 100μJ. (a) spherical, (b) flake and (c) parallelepiped. Open circles: data points, solid lines: numerical fits to the data points.

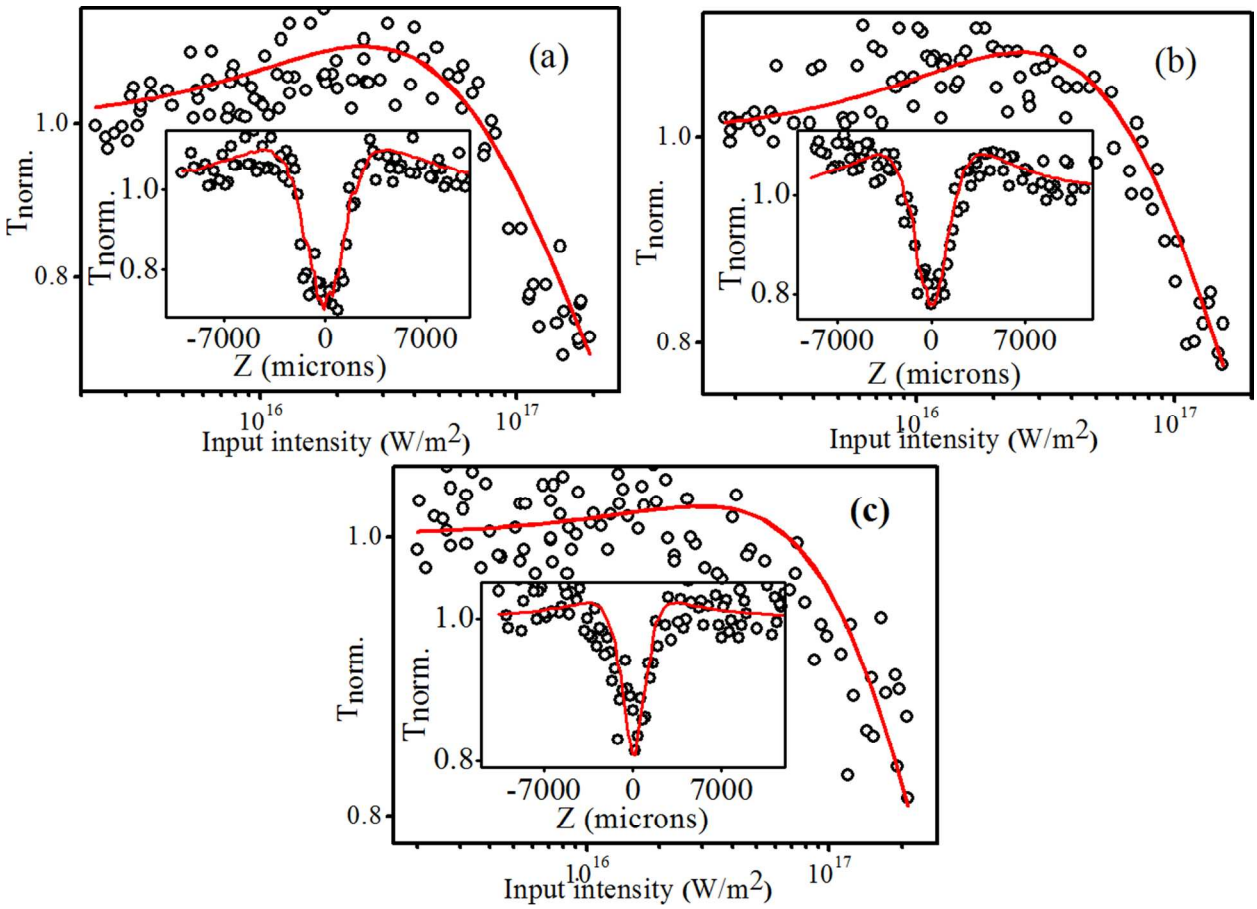

Figure 6. Open aperture Z-scans (inset) and optical limiting curves for the CdO nanomorphotypes for 800nm, 100fs laser pulse excitation at laser pulse energy of 10μJ. (a) spherical, (b) flake and (c) parallelepiped. Open circles: data points, solid lines: numerical fits to the data points.

In the limited range of pulse energies used, we could observe a clear dependence of the nonlinear absorption coefficient on input pulse energy. The variation of β_{eff} with respect to input fluence indicates that the real mechanism behind the nonlinear optical absorption in the present materials is effective two-photon absorption (2PA), originating from sequential excited state absorption (ESA) involving real intermediate states. In genuine 2PA the intermediate transition states

involved is virtual and the 2PA coefficient is a constant independent of incident laser fluence. In such a case β_{eff} is a constant indicating that there is only a negligible change or no considerable change in ground state population due to the absorption. Therefore the corresponding nonlinear absorption coefficient can be considered as a material constant for a given wavelength and fluence. However a change in β_{eff} with input fluence will be evident when there is a substantial change in the ground state population due to heavy absorption. A strong excited state absorption (ESA) depletes the ground state population significantly so that the absorption coefficient is no longer a constant. In CdO sphere, flakes and parallelepiped morphologies the normalized transmittance drops to 0.18, 0.31 and 0.37 respectively. This indicates, CdO spheres have more nonlinear optical absorption and hence higher beta effective value compared to others. In optical limiting measurements, the limiting threshold, which is defined as the input fluence at which the normalized transmittance drops to 50% of the linear transmittance, is an important parameter. Materials which have lower limiting thresholds show maximum optical limiting performance. The optical limiting threshold values calculated for ns excitation is 3.5J/cm^2, 11.5J/cm^2, 13 J/cm^2 corresponding to spherical, flake and parallelepiped morphotypes respectively, whereas the same for fs excitation is even higher. Comparing the optical limiting properties of CdO nanomorphotypes, we can conclude that the optical limiting property changes as the morphology is varied from nanosphere to nanoparallelepiped. The exact reason for change in the nonlinear optical behavior with morphology is not clearly understood, however there is previous literature suggesting that the size and shape of the nanoparticles will strongly affect the nonlinear optical behavior.[26-28] For a spherical nanostructure, the general relation for determining the ratio between surface area to volume (S/V) is 3/R (i.e.3:R) and for the case of parallelepiped structure, it is expressed as 6/L (i.e.6:L) where R and L are particle size dimensions. In the

present case nanosphere has lesser size than the remaining morphologies and hence, the nanospheres possess maximum surface to volume ratio. Since nanoflakes are similar to parallelepiped shape with one of the dimensions very small, their surface to volume ratio will lie between that of nanosphere and nanoparallelepiped structures. Due to the higher surface to volume ratio, there is maximum density of the distribution of atoms on the surface of nanostructures. Hence stronger size selective quantum confinement effect is possible in spherical morphotypes than that in flake and parallelepiped structures. This creates different discrete real intermediate transition states in the nanomaterials. The real intermediate levels depend on the strength of confinement effect occurring in the morphotypes. These levels form a band of real intermediate transition levels promoting excited state absorption (ESA). Due to the stronger confinement, maximum optical nonlinearity occurs in spherical nanomorphotypes. The surface area analysis (BET) results given in Table 4 strongly support our claim stated above. We have compared the nonlinear absorption coefficient(β_{eff}) and optical limiting threshold values previously reported for various other nano morphotypes. The nonlinear absorption coefficient for Te nanowires is the order of 10^{-11} whereas it is 10^{-10} for Ag_2Te nanowires [29], 10^{-11} for Bi nanorods [30], 10^{-11} for ZnO nanoparticles [31] and 10^{-11} for C_{60}[38]. Closely comparing the value of β_{eff} and optical limiting threshold of the present sample with the various Nanomaterials previously reported, we can ascertain that the CdO nanomorphotype is a superior material in respect of optical limiting efficiency. From these observations we can conclude that the obtained CdO nanomorphotype structures have a significantly higher optical limiting efficiency. Hence these nanomorphotypes have potential applications in devices for optical limiting, optical switching, pulse shaping, pulse compression and optical diode action.

2.5 Brunauer-Emmett-Teller (BET) analysis: The BET theory was developed by Stephen Brunauer, Paul Emmett and Edward Teller.[32] It is an extension of the Langmuir theory developed by Irving Langmuir.[33] Typically BET surface area mean multi-layer adsorption, but Langmuir refers to monolayer adsorption. BET analysis is used to determine the precise specific surface area estimation of materials by nitrogen multilayer adsorption measured as a function of relative pressure using a fully automated analyzer. The technique includes external area and pore area evaluation to determine the total specific surface area in m^2/g. It yields significant information in studying the effects of surface porosity. Barrett-Joyner-Halenda (BJH) technique is also used to determine the pore area and specific pore volume using adsorption and desorption techniques.[34] The BET, BJH and Langmuir analysis of all morphotypes are carried out by using surface area analyzer (Micromeritics Gemini 2375 V5.01, USA). The basic BET adsorption isotherm equation used in the analysis is [35-37]

$$\frac{1}{V_a\left[\frac{P_o}{P}-1\right]} = \frac{(C-1)P}{V_m C P_o} + \frac{1}{V_m C} \qquad (4)$$

Where P (Pascals) is the partial vapour pressure of adsorbate gas in equilibrium with the surface at 77K, , P_o the saturated pressure of adsorbate gas (Pascals), V_a the volume of gas adsorbed at standard temperature and pressure (STP) in milliliters, V_m the volume of gas adsorbed at STP to produce an apparent monolayer on the sample surface (milliliters) and C is the dimensionless constant that is related to the entropy of adsorption of the adsorbate gas on the powder sample. The BET and Langmuir Surface Area plot are presented in Fig. 7a and 7b respectively. These plots are linear with positive slope in the approximate relative pressure range 0.05 to 0.3. The slope and y-intercept is obtained by using least squares regression method. The BET analysis reveals that the maximum surface area is obtained in the case of spherical shape and the surface

area of flakes structure is in between spherical and parallelepiped nanostructures. All the surface area measurements are given in Table 4.

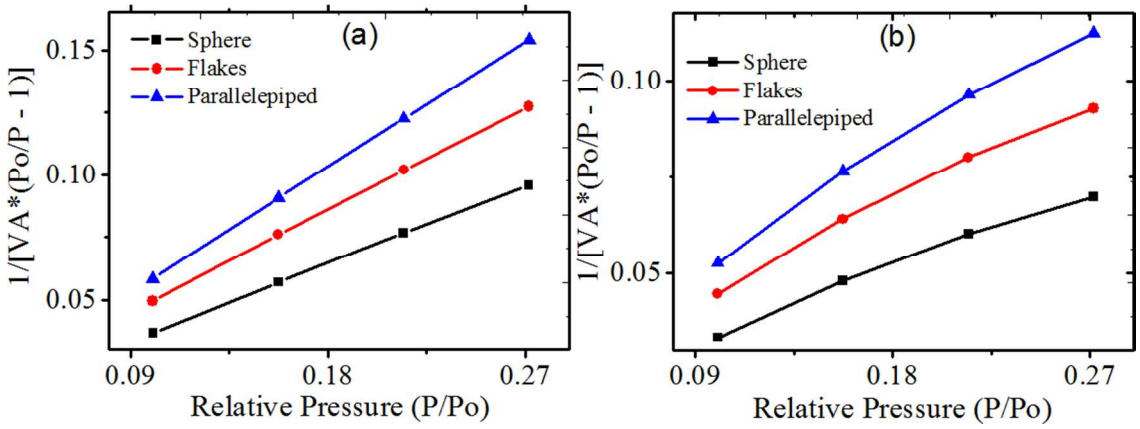

Figure 7. Surface area analysis. (a) BET Surface Area curve and (b) Langmuir Surface Area plot.

Table. 4 Parameters obtained from BET Surface area analysis using eq. 4.

Surface Area analysis	Sphere	Flakes	Parallelepiped
Single Point Surface Area (m^2/g)	12.3464	9.2851	7.6702
BET Surface Area (m^2/g)	12.5955	9.5109	7.7606
Langmuir Surface Area (m^2/g)	20.4812	15.5189	12.5074
Micropore Area (m^2/g)	0.6818	0.2945	0.8439
External Surface Area (m^2/g)	11.9137	9.2165	6.9167
Micropore Volume (cm^3/g)	0.000233	0.000055	0.000380
BJH Adsorption Average Pore Diameter (A)	74.0469	67.1888	76.9408

3. EXPERIMENTAL SECTION

3.1 Chemicals: We have introduced a novel chemical route for fabricating CdO nanospheres, flakes and parallelepiped nano morphotypes from $Cd(OH)_2$ precursor synthesized through chemical precipitation using $(CH_3COO)Cd.2H_2O$ and NaOH as starting materials. All chemicals used in the experiment were of analytical reagent (AR) grade with 99.99% purity purchased from Merck India Ltd.

3.2 Analysis techniques: The crystal structure of the samples is evaluated using X-ray diffraction analysis (Bruker AXS D8 Advance) with X-ray source Cu Ka1, Wavelength 1.5406 A°. Sample morphologies are studied using high resolution transmission electron microscope (JEM-2100, 200Kv, Jeol). The fundamental optical band gap, which is useful to nonlinear optical analysis, has been investigated through optical reflection spectroscopy (T90+UV/Vis spectrometer).

3.3 Synthesis of CdO Spherical nanoparticles: CdO nanosphere is synthesized from a precursor product obtained by the addition of 0.1M NaOH solution drop wise into 0.1M $(CH_3COO)Cd.2H_2O$ solution in double distilled water. By the addition of NaOH the entire solution becomes milky turbid due to the formation of $Cd(OH)_2$ precursor. The obtained white precursor is separated using centrifugation, followed by washing with distilled water and ethanol several times and it is then dried at 60^0 C for 4 hours. Yellowish CdO nanosphere is obtained by annealing the precursor at 500^0 C for 5 h in air.

3.4 Synthesis of CdO nanoflakes and nanoparallelepiped morphologies: For preparing the nanoflakes and nanoparallelepiped morphotypes, a specific amount of $C_6H_{15}NO_3$ (TEA), (1 ml TEA is added to each 100 ml solvent) is added to the same precursor and the mixture is poured in to a Teflon lined stainless steel autoclave. The autoclaves is fired at 200^0 C for 8

hours to for the formation of $Cd(OH)_2$ nanoflakes and 24 hours for the formation of $Cd(OH)_2$ parallelepiped nanostructures which is finally cooled down naturally to room temperature. The end products are washed, dried and annealed exactly in the same way as for CdO spherical nanoparticles.

3.5 Growth mechanism: The growth mechanism for the formation of various morphologies of CdO nanostructures is represented in Fig.8. Here the nanostructures have been fabricated through chemical precipitation and hydrothermal methods. The shape of materials in chemical precipitation process is usually spherical and we have little control on the morphology in this process. Hydrothermal process is one in which we have good control on morphology of the material. The hydrothermal processing can be defined as a heterogeneous reaction in the presence of aqueous solvents under high pressure and temperature. The working temperature, time of firing and concentration of capping agent are three important parameters for controlling the morphology of a particular material in hydrothermal reaction.

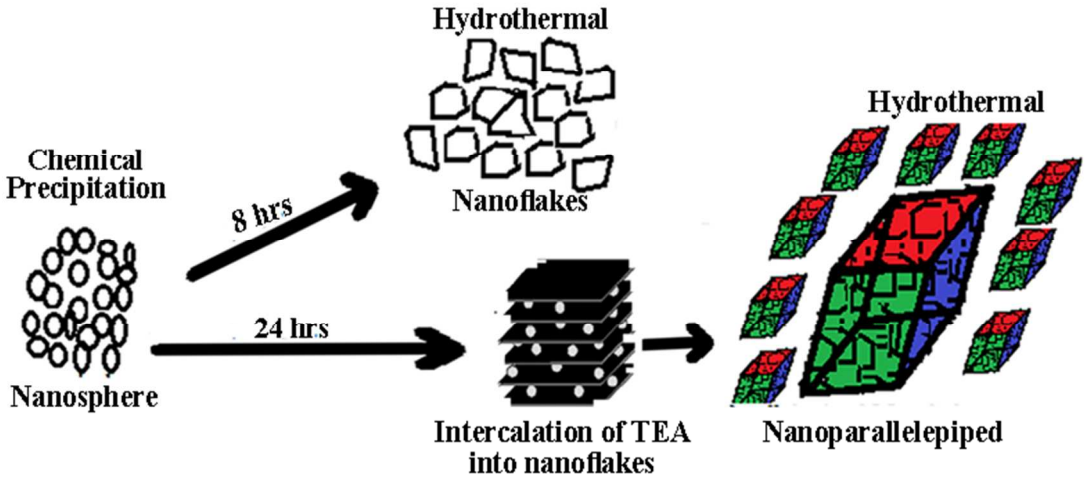

Figure 8. Schematic representation of growth profiles.

Generally autoclaves are used for providing constant pressure and temperature to the reactant. In the present synthesis, nanosphere is formed through the chemical precipitation method. The reactants $(CH_3COO)Cd.2H_2O$ and NaOH are dissolved in double distilled water to form Cd^{2+} and OH^{2-} ions. The Cd^{2+} and OH^{2-} ions are combined in bottom up approach to form the $Cd(OH)_2$ spherical particles. The entire reaction is too slow and it is carried out at atmospheric pressure and room temperature; therefore the atoms have an opportunity to attain the most stable spherical shape/morphology in the reaction. In the next stage nanoflakes are fabricated from $Cd(OH)_2$ nanosphere which under goes hydrothermal treatment at 200^0 C for 8 hrs with $C_6H_{15}NO_3$ employed as capping agent. The capping agent $C_6H_{15}NO_3$ encloses $Cd(OH)_2$ nanosphere and uniformly transmit the pressure existing inside the autoclave to each of the particle. Due to this huge pressure some lattice strain is skewed out through weak regions of $C_6H_{15}NO_3$ enclosure which results in breaking of the enclosure and formation of fish scale like structure called $Cd(OH)_2$ nanoflakes. The most of the nanoflakes have hexagonal morphology which is clearly visible in our HRTEM analysis. In the case of parallelepiped morphotype the same $Cd(OH)_2$ nanosphere is admitted to hydrothermal reaction for 24 hrs at 200^0 C. After the formation of $Cd(OH)_2$ nanoflakes (beyond 8 hrs of firing) the intercalation of $C_6H_{15}NO_3$ in to different nanoflakes, generates bundles of nanoflakes formed by layer by layer stacking of flakes. At the same time $C_6H_{15}NO_3$ enclosing the bundles provide high pressure to it. Due to this high pressure bundles of nanoflakes are slipped slightly to form $Cd(OH)_2$ parallelepiped morphology. The exact crystalline phases of CdO are created by annealing the samples after the hydrothermal reaction at 500^0 C for 5 hrs.

4. CONCLUSIONS

In summary, we have synthesized CdO crystalline nanosphere, nanoflakes, and nanoparallelepiped morphotypes by hydrothermal route and carried out ns and fs optical nonlinearity studies using open aperture z-scan technique. The crystalline nature, versatile morphology and particle size are analyzed by XRD and High resolution transmission electron microscopy. The measured nonlinear optical absorption coefficients reveal that the dominant nonlinear absorption mechanism is effective two-photon absorption which originates mainly from excited state absorption. The magnitude of two-photon absorption coefficient is calculated and is found to be in the range of 10^{-10}m/W for ns and 10^{-15} m/W for fs. The optical nonlinearity is dependent on the size and shape of the nanomaterials. The claim of morphology dependent nonlinear optical absorption is strongly supported by BET surface area analysis. The maximum nonlinear optical absorption coefficient and minimum optical limiting threshold values are obtained for CdO spherical shapes.

ACKNOWLEDGEMENT

The authors thank the team members of match!2 crystal phase matching software developers for allowing the authors to download the software for Rietveld analysis, NIIST Thiruvananthapuram (BET analysis), SAIF Cochin (XRD and SEM analysis) and NEHU Shillong (TEM analysis) for providing facility for analyzing the samples.

REFERENCES

1. M.A. El-Sayed, Some Interesting Properties of Metals Confined in Time and Nanometer Space of Different Shapes. *Acc. Chem. Res*. 2001, **34**, 257-264.

2. N. R. Jana, L. Gearheart, C. J. Murphy, Wet Chemical Synthesis of High Aspect Ratio Cylindrical Gold Nanorods. *Chem. Commun.* 2001, **7**, 617–618.

3. Tz-Jun Kuo, H. Michael Huang, Gold-Catalyzed Low-Temperature Growth of Cadmium Oxide Nanowires by Vapor Transport. *J. Phys. Chem. B*. 2006**, 110**, 13717-13721.

4. V. Eskizeybek, A. Avci, M. Chhowalla, Structural and optical properties of CdO nanowires synthesized from $Cd(OH)_2$ precursors by calcinations. *Cryst. Res. Technol.* 2011**, 46**, 1093-1100.

5. Tandra Ghoshal, Soumitra Kar, Subhadra Chaudhuri, Synthesis of nano and micro crystals of $Cd(OH)_2$ and CdO in the shape of hexagonal sheets and rods. *Applied Surface Science*. 2007, **253,** 7578–7584.

6. Maryam Lashanizadegan, Hoda Mirzazadeh, A facile method to prepare CdO-Mn3O4 nanocomposite. *J. Ceramic Processing Research.* 2012**, 13**, 389-391.

7. S.W. Chung, J.Y. Yu, J.R. Heath, Silicon nanowire devices. *Appl. Phys. Lett*. 2000**, 76**, 2068-2070.

8. Cuscó. R, Ibáñez. J, Domenech-Amador. N, Artús. L, Zúñiga-Pérez. J, Muñoz-Sanjosé V, Raman scattering of cadmium oxide epilayers grown by metal-organic vapor phase epitaxy. *J. Appl.Phys*. 2010**, 107**, 063519.

9. Sathish Reddy, B.E. Kumara Swamy, Umesh Chandra, B.S. Sherigara, H. Jayadevappa, Synthesis of CdO nanoparticles and their modified carbon paste electrode for determination of dopamine and ascorbic acid by using cyclic voltammetry technique. Int. *J. Electro chem. Sci.* 2010, **5**, 10 – 17.

10. Y.W. Wang, C.H. Liang, G.Z. Wang, T. Gao, S.X. Wang, J. C. Fan, Preparation and Characterization of Ordered Semiconductor CdO Nanowire Arrays. *J. Mater Sci Lett*. 2001**,** **20**, 1687-1689.

11. Jayakrishna Khatei, C.S. Suchand Sandeep, Reji Philip, K.S.R. Koteswara Rao, Near-resonant two-photon absorption in luminescent CdTe quantum dots. *J. Appl. Phys.Lett.* 2012**,** **100**, 081901.

12. A.R. Barik, K.V. Adarsh , Ramakanta Naik, C.S. Suchand Sandeep, Reji Philip, Donghui Zhao, Himanshu Jain, Photoinduced transparency of effective three-photon absorption coefficient for femtosecond laser pulses in $Ge_{16}As_{29}Se_{55}$ thin films. *J. Appl. Phys. Lett.* 2011**,** **98**, 201111.

13. D. Ambika, Viswanathan Kumar, C.S. Suchand Sandeep, Reji Philip, Tunability of third order nonlinear absorption in PLZT thin films. *J. Appl. Phys. Lett.* 2011**,** **98**, 011903.

14. Y.W. Jun, Y.Y. Jung, J. Cheon, Characterization of Semiconductor Heterostructures and Nanostructures. *J. Am. Chem. Soc.* 2002**,** **124**, 615 -619.

15. T. Ghoshal, S. Kar, S. Chaudhuri, Synthesis of micro and nanostructures of $Cd(OH)_2$ and CdO in shape of hexagonal sheets and rods. *J. Appl surface science.* 2007**,** **253**, 7578-7584.

16. Wen-Shou Wang, Liang Zhen, Cheng-Yan Xu, Wen-Zhu Shao, Aqueous Solution Synthesis of $Cd(OH)_2$ Hollow Microspheres via Ostwald Ripening and Their Conversion to CdO Hollow Microspheres. *J. Phys. Chem. C***.** 2008**,** **112,** 14360-14366.

17. A.M. Nasser, Barakat, Salem Al-Deyab, Hak Yong Kim, Synthesis and study of the photpluminescence and optical characterization of Cd/CdO nanorods prepared by the electrospinning process. *J. Materials letters,* 2012**, 66**, 225-228.

18. Zhiyong Jia, Yiwen Tang, Lijuan Luo, Bihui Li, Shape-Controlled Synthesis of Single-Crystalline $CdCO_3$ and Corresponding Porous CdO Nanostructures. *J. Crystal growth and Design.* 2008**, 8**, 2713-2715.

19. Q. Chang, Enhanced Hydrogen Production over C-Doped CdO Photocatalyst in Na_2S/Na_2SO_3 Solution under Visible Light Irradiation. *Int. J. Photo energy*. 2012**,** **10**.1155//857345.

20. H. Pan, W. Chen, Y. P. Feng, W. Ji, Optical limiting properties of metal nanowires. *J. Appl. Phys. Lett.* 2006**, 88**, 223106.

21**.** Q. Chang, C. Chang, X. Zhang, H. Ye, G. Shi, W. Zhang, Y. Wang, X. Xin, Y. Song, Enhanced optical limiting properties in suspensions of CdO nanowires. *J. Opt. Commun.* 2007, **274**, 201-205.

22. N. Venkatram, D. Narayana Rao, M. A. Akundi, Nonlinear absorption, scattering and optical limiting studies of CdS nanoparticals. *J. Optics Express.* 2005**, 13**, 867-872.

23. M. Sheik Bahae, A. A. Said, T. M. Wei, D. J. Hagan, E. W. Vanstryland, Sensitive Measurement of Optical Nonlinearities Using a Single Beam. *IEEE J. Quantum Electron.* 1990**, 26**, 760-769.

24. W. L. Jia, E. P. Douglas, Optical limiting of semiconductor nanoparticles for nanosecond laser pulses. *J. Appl. Phys. Lett.* 2004**, 85**, 6326-6328.

25. Reji Philip, Panit Chantharasupa, Huifeng Qian, Rongchao Jin, Jayan Thomas, Evolution of Nonlinear Optical Properties: From Gold Atomic Clusters to Plasmonic Nanocrystals. *J. Nano Lett.* 2012**, 12**, 4661-4667.

26**.** Paresh Chandra Ray, Size and Shape Dependent Second Order Nonlinear Optical Properties of Nanomaterials and Their Application in Biological and Chemical Sensing, *J. Chem Rev.* 2010**, 110**, 5332-5365.

27**.** Ramakrishna Podila, Benoy Anand, Palmer West, Reji Philip, S. Siva Sankara Sai, Jian He, Malcolm Skov, Shiou-Jyh Hwu, Sumanta Tewari, Apparao Rao. M, Evidence for surface states in pristine and Co-doped ZnO nanostructures: magnetization and nonlinear optical studies. *J. Nanotechnology*. 2011, **22**, 095703.

28**.** O. Sánchez-Dena, Size-and shape-dependent nonlinear optical response of Au nanoparticles embedded in sapphire. *J. Optical Material Express*. 2014, **4**, 92-100.

29. C.S. Suchand Sandeep, A.K. Samal, T. Pradeep, Reji Philip, Nonlinear optical transmission measurements of Te and Ag_2Te nanowires at 532 and 1064 nm show that they are potential broadband optical limiters. *J. Chemical Physics Letters.* 2010**, 485**, 326-330.

30. S. Sivaramakrishnan, V. S. Muthukumar, S. Sivasankara Sai, S. Venkataramaniah, Nonlinear optical scattering and absorption in bismuth nanorods suspensions. *J. Appl. Phys.Lett.* 2007**, 91**, 093104.

31. R. Sreeja, R. Reshmi, G. Manu, M.K. Jayaraj, Determination of third-order optical absorptive nonlinearity of ZnO nanoparticles by Z-scan technique. *Proc. SPIE,* 2008**, 7155**, 715521.

32. Brunauer S, Emmett P H & Teller E, Adsorption of gases in multimolecular layers, *J. Am. Chem. Soc,* 1938, 60, 309-319.

33. I. Langmuir, The dissociation of hydrogen into atoms. [part ii.] calculation of the degree of dissociation and the heat of formation, *J. Am. Chem. Soc,* 1915, 37, 417-458.

34. E. P. Barrett, L. G. Joyner, P. P. Halenda, The determination of pore volume and area distributions in porous substances. I. Computations from nitrogen isotherms, *J. Am. Chem. Soc,*1951, 73, 373–380.

35. Itodo A. U, Itodo H. U, Gafar M. K, Estimation of Specific Surface Area using Langmuir Isotherm Method, *J. Appl. Sci. Environ. Manage,* 2010, **14**, 141 – 145.

36. Komban Rajesh, Palantavida Shajesh, Biji Pullithadathil, Krishna Gopakumar Warrier, High surface area mesoporous Nanocrystalline lanthanum phosphate nanorods through a sol-gel process Effect of alcohol washing on a non-oxide gel. *Microporous and Mesoporous Materials*, 2008, **116**, 693-697.

37. Sasidharan Sankar , Krishna Gopakumar Warrier, Rajesh Komban, High surface area neodymium phosphate nano particles by modified aqueous sol-gel method, *Materials Research Bulletin* , 2011, **46**, 2373-2377.

38. J.Wang, W.J.Balu, Inorganic and hybrid nanostructures for optical limiting, *J.Opt. A Pure Appl. Opt*, 2009, **11**, 0244001.